THE ASTROPHYSICAL JOURNAL, 198:163–182, 1975 May 15

HIGH-ENERGY GAMMA-RAY RESULTS FROM THE SECOND SMALL ASTRONOMY SATELLITE

C. E. FICHTEL, R. C. HARTMAN, D. A. KNIFFEN, D. J. THOMPSON, AND G. F. BIGNAMI*
NASA/Goddard Space Flight Center, Greenbelt, Maryland
AND
H. ÖGELMAN, M. E. ÖZEL, AND T. TÜMER
Middle East Technical University, Ankara, Turkey
Received 1974 October 7

ABSTRACT

A high-energy (>35 MeV) γ-ray telescope employing a 32-level wire spark-chamber system was flown on the second Small Astronomy Satellite (SAS-2). The high-energy galactic γ-radiation is observed to dominate over the general diffuse radiation along the entire galactic plane and is seen to be most pronounced in a region from $l^{\rm II} = 335°$ to $l^{\rm II} = 40°$. When examined in detail, the longitudinal and latitudinal distributions seem generally correlated with galactic structural features, and particularly with arm segments. On the basis principally of its angular distribution and magnitude, the general high-energy γ-radiation from the galactic plane seems to be explained best as resulting primarily from cosmic-ray interactions with interstellar matter. From the study of six different regions of the sky with $|b^{\rm II}| > 30°$, there appears to be a uniform celestial γ-radiation, as suggested by earlier results, especially Kraushaar *et al.* Over the energy range from about 35 MeV to 170 MeV, the differential spectrum has the form

$$\frac{dJ}{dE} = (2.7 \pm 0.5) \times 10^{-7}\left(\frac{E}{100}\right)^{-2.4\pm0.2} \gamma\text{-rays cm}^{-2}\text{ sr}^{-1}\text{ s}^{-1}\text{ MeV}^{-1},$$

where E is expressed in MeV. If the apparent flattening of the spectrum in the 0.6–10 MeV region observed in other experiments is verified, the high-energy results reported here, when combined with the lower-energy data, suggest a cosmological origin for this radiation. In addition to the general galactic emission, high-energy γ-radiation was seen from the Crab Nebula (a significant fraction of which is pulsed at the radio pulsar frequency), Vela X (a supernova remnant whose high-energy γ-radiation possibly provides the first direct experimental evidence associating cosmic rays with supernovae), the general region ($15° < b^{\rm II} < 30°$, $340° < l^{\rm II} < 20°$), and a region a few degrees north of the galactic plane around 190° to 195° in $l^{\rm II}$. Several upper limits to high-energy γ-ray fluxes were also set, including among others, above 100 MeV: 1.0×10^{-6} for the Small Magellanic Cloud, 9.5×10^{-7} for Sco X-1, 2.5×10^{-6} for 3C 120, 1.0×10^{-6} for M87, and 1.1×10^{-6} for Cas A in units of photons ($E > 100$ MeV)/(cm^2 s).

Subject headings: cosmic rays — Crab Nebula — galactic structure — gamma rays — pulsars — supernova remnants

I. INTRODUCTION

High-energy γ-ray astronomy has long been known to hold potentially great rewards because of its ability to reveal the dynamic, high-energy processes in our Galaxy and the Universe. The first certain detection of celestial γ-rays came from a satellite experiment flown on OSO-3. With this detector, Kraushaar *et al.* (1972) observed the emission of γ-rays with energies above 50 MeV from the galactic disk with a peak intensity toward the galactic center. However, the limited spectral and spatial resolution of this pioneering experiment left many questions unanswered. Four other early satellite high-energy γ-ray experiments were those on COSMOS-208 (Bratolyubova-Tsulukidze *et al.* 1971), COSMOS-264 (Galper *et al.* 1973), OGO-5 (Hutchinson *et al.* 1971), and OSO-3 (Badhwar, Kaplon, and Valentine 1974). During the last decade, there have also been numerous attempts to detect high-energy γ-radiation with balloon-borne experiments, but these have been seriously hampered by the high level of atmospheric γ-rays due to cosmic-ray interactions in the atmosphere.

The experiment is a picture-type high-energy (>35 MeV) γ-ray telescope using a 32-level wire spark-chamber and flown on the second NASA Small Astronomy Satellite (SAS-2). It has the advantages of providing a wide field of view (full width half-maximum angle of 35°), but still permitting a few degrees angular resolution for individual γ-rays and providing positive identification of the γ-rays, as well as an estimate of their energy.

The data reported in this work includes the first 17 weeks of exposure which covers all the observed regions of the galactic plane as well as six regions away from the plane. Results fall into three subject areas: the relatively intense component from the galactic plane with its hard energy spectrum; the diffuse, apparently extragalactic radiation; and localized

* ESRO Postdoctoral Fellow on leave from LFCTR, Istituto di Fisica dell'Università di Milano, Italy.

sources. A discussion of each of these will follow the experiment description.

II. THE EXPERIMENT

a) *Gamma-Ray Telescope Description*

A schematic diagram of the γ-ray telescope flown on SAS-2 is shown in Figure 1. The spark chamber assembly consists of 16 wire spark-chamber modules with a magnetic core readout system above a set of four central plastic scintillators and another 16 modules below these scintillators. Thin tungsten plates, 0.03 radiation length-thick, are interleaved between the spark-chamber modules, which have an active area of approximately 640 cm^2. The large number of thin tungsten plates and spark chambers serve a dual purpose: first, to provide material for the γ-ray to be converted into an electron pair which can then be clearly identified and from which the arrival direction of the γ-ray can be determined; and second, to provide a means of determining the energy of the electrons in the pair by measuring their Coulomb scattering. The array of four plastic scintillator tiles (B_i) in the center of the spark chamber and the four directional Cerenkov detectors (C_i) at the bottom constitute four independent counter coincidence systems. A single-piece plastic scintillator dome (A) surrounds the spark-chamber system, except at the bottom of the experiment, to discriminate against charged particles. The logic $\bar{A}B_iC_i$ is used to select γ-rays entering from the top of the telescope, converting into an electron pair in the upper half of the chamber, and subsequently triggering one of the four counter pairs. A digitized spark chamber "picture" of a γ-ray–induced electron pair is shown in Figure 2.

The energy threshold is about 30 MeV. The energy of the γ-ray can be measured up to about 200 MeV, and the integral flux above 200 MeV can be determined. A more complete discussion of the SAS-2 γ-ray telescope is given by Derdeyn *et al.* (1972).

b) *Satellite Characteristics*

The γ-ray telescope is mounted at its base to the SAS-2 spacecraft, which provides electrical power, commands, data recording, telemetry, attitude control, and aspect sensing. SAS-2 is spin stabilized with magnetic torquing to allow pointing to any region of the sky. The spacecraft aspect is monitored by two separate sets of sensors. A digital solar aspect detector and a three-axis set of magnetometers together are capable of providing aspect accuracy of about 0°.3. Star sensor data can refine the accuracy to about 0°.2. Absolute time of arrival of individual γ-rays is determined to an accuracy of ± 1 ms, the principal uncertainty resulting from the spacecraft clock and the event timing signal. A more detailed description of the SAS-2 spacecraft has been given by Townsend (1969).

The low fluxes involved in the study of celestial γ-radiation make it desirable that the collection of useful satellite data be as complete as possible. These considerations led to the choice of a low Earth equatorial orbit (2° inclination with an apogee of 610 km and a perigee of 440 km), and an orbital period of 95 minutes.

The observation program was planned to provide an exposure to the entire sky within 1 year of operation, with early emphasis being placed on the galactic plane. Some early exposures to regions of intermediate and high galactic latitudes were included for study of possible discrete sources and of the diffuse γ-radiation. Based on estimated counting rates, an optimum viewing period of one week was chosen for each region of the sky at which the telescope was pointed. The satellite was launched on 1972 November 15, and the experiment was activated on 1972 November 19. On 1973 June 8, a failure in the input portion of the low-voltage power supply ended the collection of data from SAS-2. At that time approximately 55 percent of the sky had been examined, including most of the galactic plane as shown in Figure 3.

c) *Data Reduction*

i) *Gamma-Ray Events*

The first step in the reduction of the experiment data is the selection of unambiguous γ-ray events from all those events which have satisfied the trigger logic of the spark chamber. For this purpose we require that the positron-negatron pair should form a distinctive picture, appearing as an inverted Y or V in at least one of the orthogonal views. The events which are eliminated fall largely into two categories. The first of these includes all events which originate in the detector walls rather than in the conversion plates. While some such events may be of γ-ray origin, their interpretation would be ambiguous. The majority of the remaining events fall into the second category—single-track events. These events are largely electrons entering through the bottom of the detector (resulting from the fact that the directional Cerenkov counter is not absolute in rejecting backward-moving particles), Compton electrons, and very high energy unresolved pairs. Since the latter cannot be unambiguously separated from the others, all single-track events are rejected, and the efficiency is determined on the basis of those γ-rays which create clearly defined pairs. Both the calibration and flight data were analyzed using the same criteria to maintain consistency of interpretation and correctly determine effective efficiencies.

Energy calculations are based on the multiple scattering of the pair electrons in the tungsten plates. The formalization for this analysis has been discussed in detail previously, but has been extended for this work to include uneven cell size as encountered when an electron does not have set core locations in some decks because of the finite spark chamber efficiency. The mathematical details of this development are presented in the Appendix. The quantitative accuracy has been verified by detailed calibrations, which will be discussed in the following section.

Gamma-ray arrival directions are based on a weighted bisector method which weights the estimated

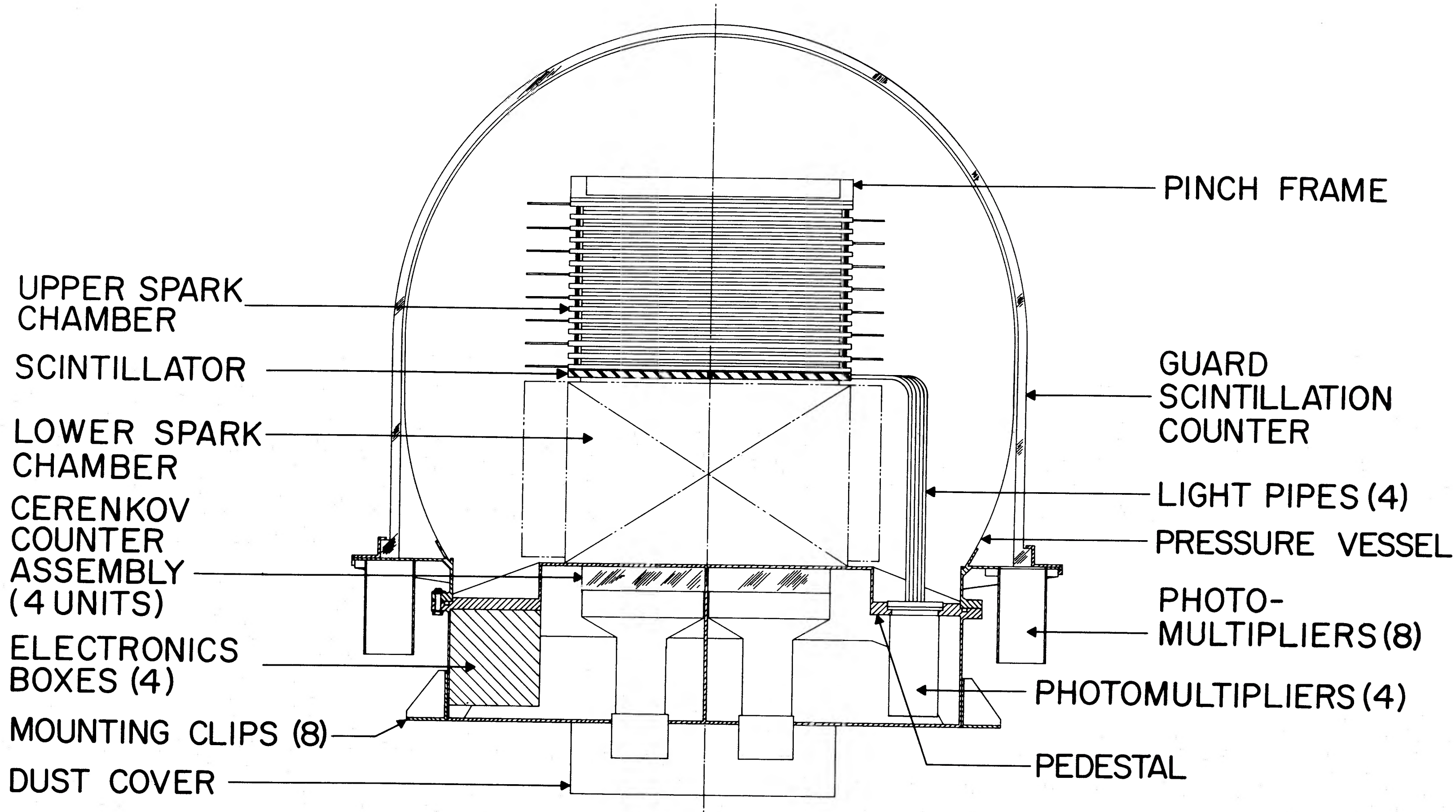

FIG. 1.—Schematic diagram of the SAS-2 γ-ray experiment (Derdeyn *et al.* 1972)

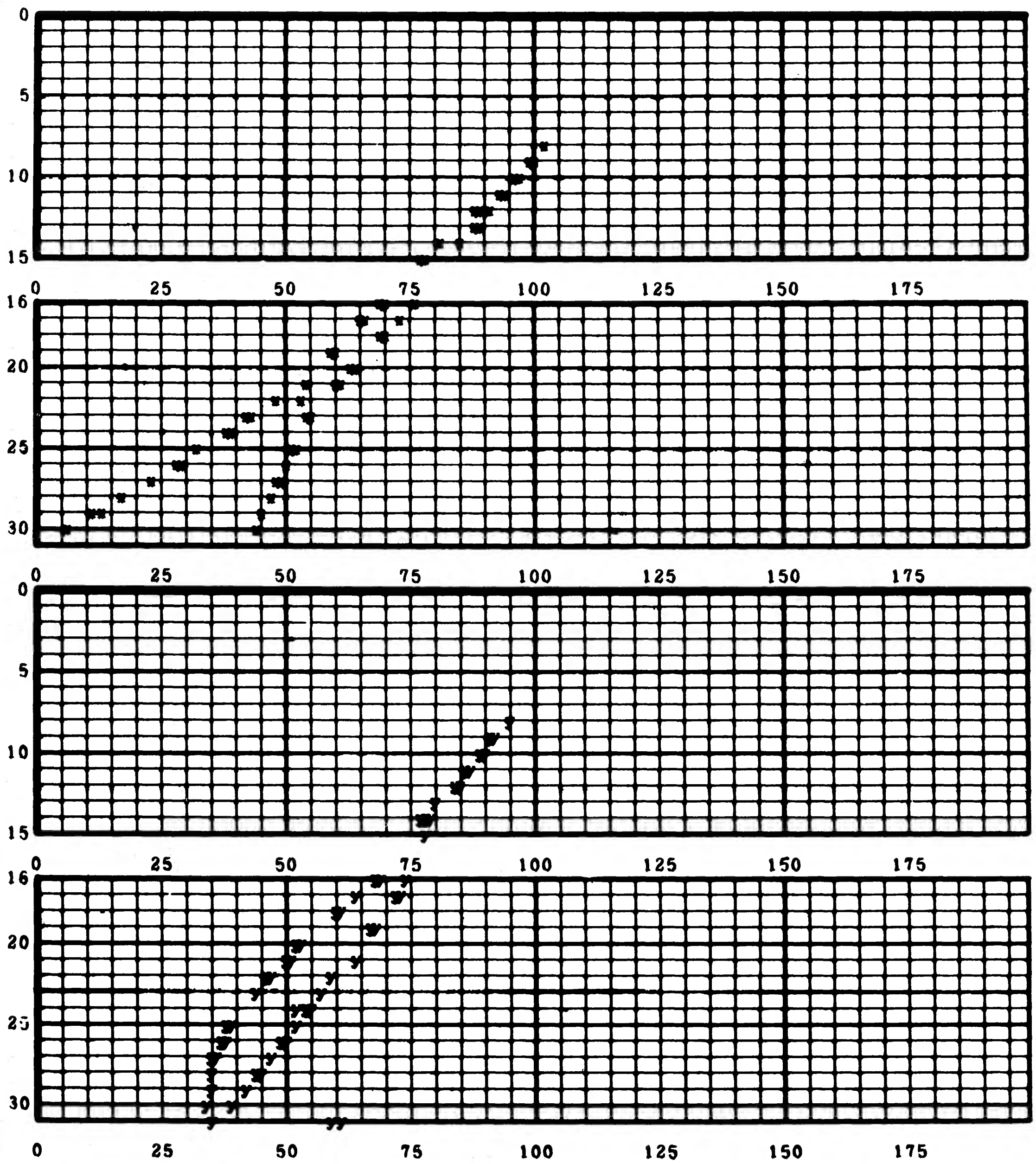

FIG. 2.—Readout display of a γ-ray pair production event in the spark chamber shown in two orthogonal views. The X's and Y's denote cores set due to the passage of charged particles in the x- and y-views, respectively. *Top two grids*, X array; *bottom two grids*, Y array. The vertical axis has been compressed by a factor of 2.7 relative to the horizontal axis. Event was 1972 December 12, $21^h22^m50^s$ 520 ms.

direction toward the higher energy electron (Fichtel *et al.* 1972). From the arrival direction in telescope coordinates, the attitude data are used to transform the apparent direction of arrival of the ambient photon into any selected celestial coordinate system. The accuracy of the directional determination will be discussed in § II*c*(ii). In the subsequent analysis only γ-rays whose arrival directions are determined to be within 90° of the vertical and 30° of the detector axis are accepted.

During the period 1972 November 19 to 1973 March 20, when the data to be discussed in this paper were accumulated, over 8000 analyzed γ-rays satisfied these angular criteria and also had measured energies greater than 35 MeV. Although some γ-rays had lower measured energies, the effective area solid angle calibration is less certain at these lower energies; therefore, a lower limit of 35 MeV has been adopted. Almost 12,000 additional analyzed γ-rays were rejected because they did not satisfy these criteria, with

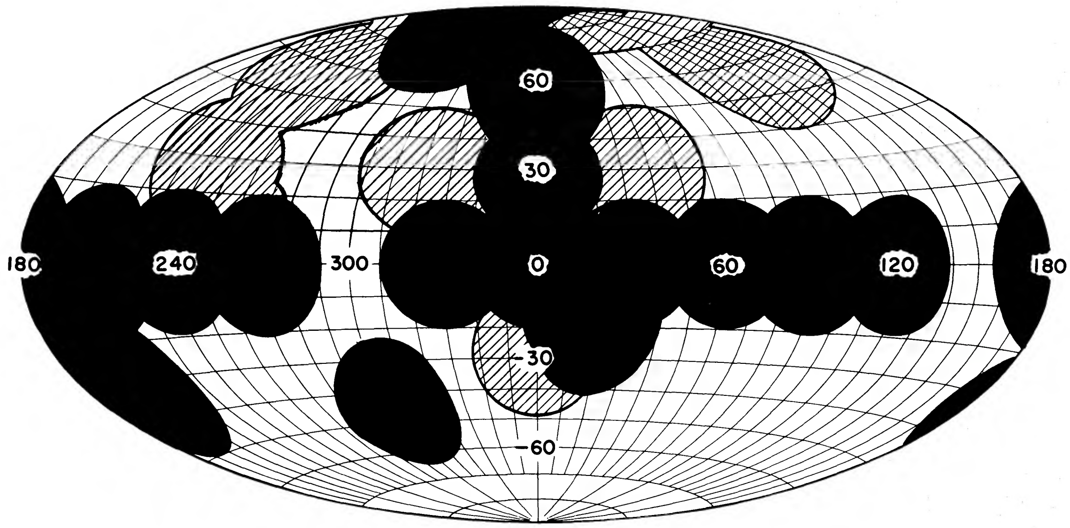

FIG. 3.—Regions of the sky viewed by SAS-2, using a circle drawn about the viewing axis with a radius corresponding to the angle at which the sensitivity for detection of γ-rays is 0.4 to 0.5 the value along the detector axis, depending on energy. The blackened regions are those used for the results of this paper.

the great majority of the rejected γ-rays having zenith angles greater than 90°—mostly near the Earth horizon angle (typically 115° with respect to the vertical) and therefore predominantly Earth albedo. For the data on which absolute fluxes were calculated and reported in this paper, the event selection was further restricted by accepting only γ-rays whose measured arrival directions were within about 25° of the detector axis because of the increased uncertainty associated with the calibrated sensitivity at wide angles.

ii) *Calibration*

An extensive program of calibration was conducted for the SAS-2 experiment using both the flight unit and an identical flight spare unit. The energy range from approximately 20 to 114 MeV was studied at the National Bureau of Standards Synchrotron (NBS), Gaithersburg, Maryland, using the γ-ray beam developed jointly by NBS and GSFC and described by Hartman *et al.* (1973). The energy range to 1000 MeV was studied at Deutsches Elektronen-Synchrotron (DESY), Hamburg, using the tagged γ-ray beam developed for the calibration of the COS-B spark-chamber telescope and described by Christ *et al.* (1974).

The γ-ray detection efficiency is shown in Figure 4, which displays the effective area as a function of energy for four incident angles with respect to the detector axis. The efficiency used is the net efficiency after both trigger probability and event acceptance criteria, discussed previously, are included. Computer Monte Carlo simulations confirming the accelerator calibrations are also included in this figure.

The angular resolution of the detector has been measured at the two facilities for the range of energies from 37 to 1000 MeV. Figure 5 gives the average deviations from the median of the distributions of the reconstituted arrival direction angles as a function of γ-ray energy. No significant difference has been found for the angular resolution when looking at γ-rays incident off the detector axis or at an angle with respect to the principal detector axis up to 15° from the vertical. The angular resolution degrades by 25–30 percent between 15° and 30°.

In addition to the calibration at NBS and DESY there were two means of estimating the detection capability of the SAS-2 γ-ray telescope in flight. These

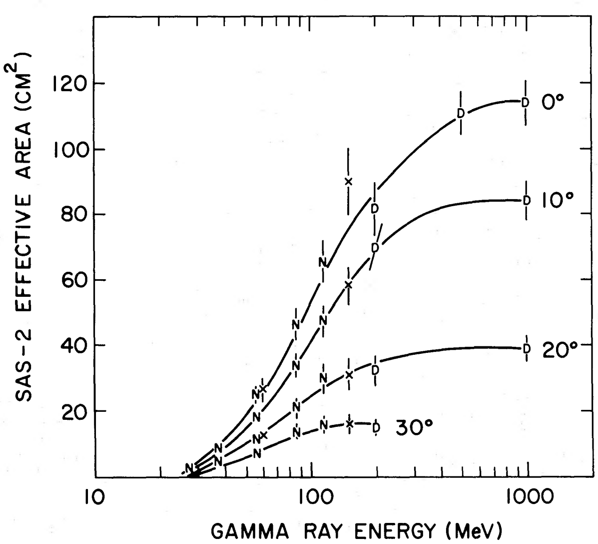

FIG. 4.—SAS-2 effective area for γ-ray detection, as a function of γ-ray energy, based on calibrations at the National Bureau of Standards (points N) and the Deutsches Elektronen-Synchrotron (points D). The points represent the fractional detection efficiency times the detector area, averaged over the surface of the detector, including all acceptance criteria for γ-rays as described in the text. The angles shown are between the beam direction and the detector axis. The solid lines are fits to the experimental data points. Also shown for comparison are sample points from a detailed Monte Carlo calculation of the detector efficiency (points X), which agrees with the calibration data.

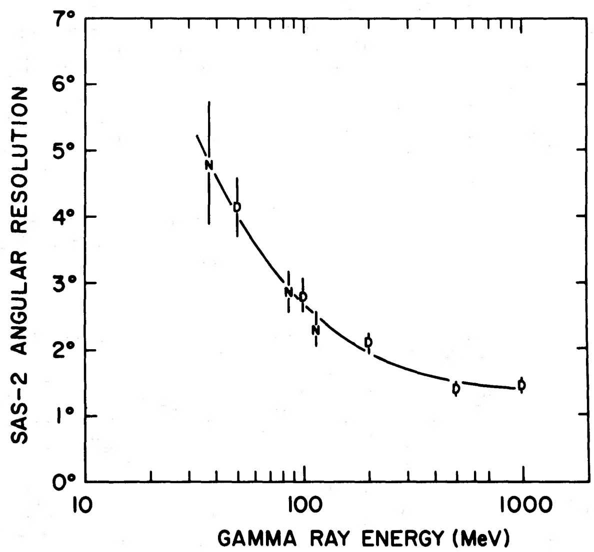

FIG. 5.—Angular resolution for the SAS-2 detector, based on calibrations at NBS (points N) and DESY (points D). The values represent the average deviation from the median of the measured gamma-ray arrival directions, evaluated separately in the two orthogonal views. The solid line is a fit to the data.

are based on the atmospheric albedo and celestial diffuse radiation. The latter made use of the data from high galactic latitudes where the diffuse radiation appears isotropic. This approach gave a postlaunch comparison of the angular response of the detector of low statistical weight, but nonetheless one which did confirm the gross features of the calibration. The atmospheric radiation measurement agreed within errors with the flux expected from previous measurements (Fichtel, Hartman, and Kniffen 1973*a*).

The method used for the individual γ-ray energy evaluation is based on the analysis of the scattering of the two tracks of the electron pair, described in the previous section and the Appendix. Figure 6 shows the distributions of estimated γ-ray energies for various incident beam energies, at 0° inclination. The spread in energy of both the NBS and DESY γ-ray beams is small compared with the detector energy resolution. It is seen that, although the energy resolution is limited, a consistent evaluation of the γ-ray energy is possible up to about 200 MeV where the method is no longer useful because of the predominance of the "reading error" in the scattering measurement.

In principle, with very good statistics the primary energy spectrum can be deduced from the measured energy distribution using a least-squares method such as that developed by Trombka and Schmadebeck (1968). In this instance statistical fluctuations dominate leading to unlikely results or effectively an indeterminate situation. If, on the other hand, the primary spectrum may be represented by the sum of simple smooth curves over the relatively small energy range of interest here (about 25 to 500 MeV), then the most likely measured spectrum can be calculated on the basis of the experimentally measured energy-dependent distribution function. It has been assumed here that

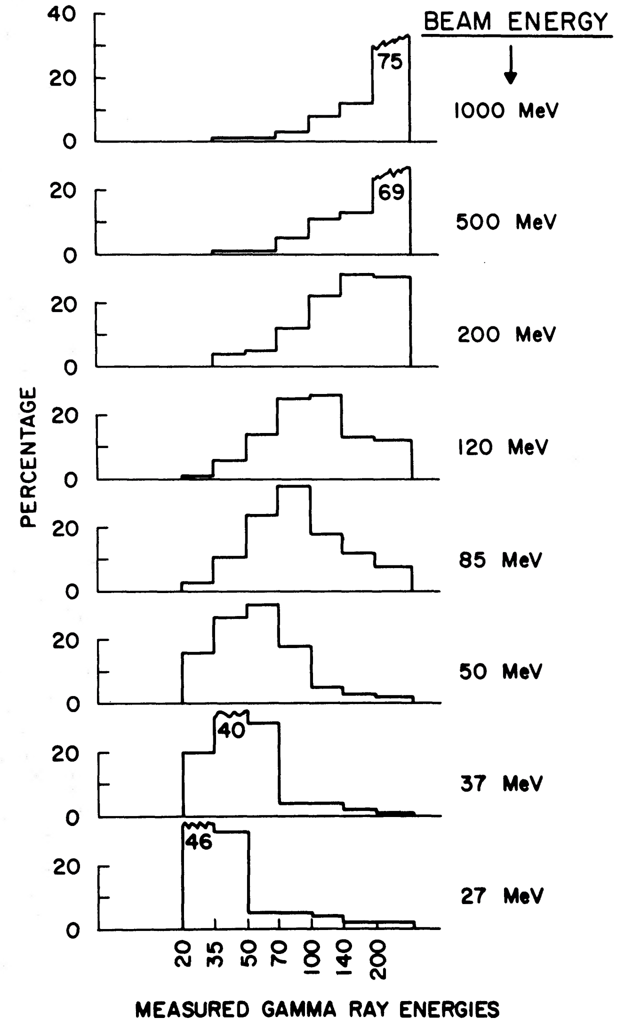

FIG. 6.—Energy measurement and resolution of the SAS-2 detector, based on calibrations at NBS and DESY. For the beam energies shown, the histograms show the percentage of γ-ray events with energies measured in each of seven energy bins. The energy measurement uses the multiple scattering technique discussed in the text.

the primary spectrum was either a power law of the form

$$dJ/dE = KE^{-n} \tag{1}$$

or a combination of this spectrum and a cosmic-ray nucleon-nucleon interaction γ-ray spectrum as calculated, for example, by Stecker (1970).

iii) *Sensitivity Calculation*

The reduction of the observed γ-ray intensity to an absolute celestial intensity or flux requires a knowledge of the relative amount of exposure to each region of the sky. In addition to an accurate determination of the detector response, this requires a knowledge of the attitude of the detector axis, the angle of the axis with respect to the Earth vertical vector, the orbital position of the satellite, and live time of the telescope, the percentage of data lost, and the status of experiment commands which affect the exposure value. A program was developed which scans the entire data base for the required input information and calculates the exposure to any desired region of the sky, taking into account earth occultation and telescope sensitivity as a function of detector axis angle.

III. EXPERIMENTAL RESULTS AND DISCUSSION

a) *Galactic Plane*

i) *Experimental Results*

Relative to the general background celestial diffuse radiation, a strongly enhanced intensity of high-energy γ-rays is observed along the entire galactic plane. The energy spectrum of this galactic-plane γ-radiation is observed to have a flatter energy spectrum than that of the diffuse celestial radiation to be discussed later in § III*b*. Galactic plane results from SAS-2, based on relatively few exposure periods and preliminary calibration, were reported by Kniffen *et al.* (1973).

The region in l^{II} from about 325° to about 40° is particularly intense, as seen in Figure 7, which shows the intensity of γ-rays above 100 MeV summed from $b^{\text{II}} = -10°$ to $b^{\text{II}} = +10°$ and plotted as a function of galactic longitude in 5° intervals. Notice particularly that the radiation from the galactic center itself is not significantly more intense than the rest of this interval. This lack of a single, strong peak in the γ-ray distribution at the center excludes the possibility of explaining the general enhancement in the region ($325° < l^{\text{II}} < 40°$) solely in terms of a theory involving a strong maximum of emission in the galactic center region.

Considering the radiation in the $330° < l^{\text{II}} < 30°$ interval, Figure 8*a* shows the angular distribution in b^{II} for γ-rays with measured energies above 100 MeV. There is clearly a relatively narrow component, which can be shown to be consistent with, or only slightly broader than, the detector resolution alone, discussed in § II*c*. In addition, there is a much broader component. The experimental points in Figure 8*a* have been compared with the sum of two curves, one with the detector angular resolution corresponding to a hard spectrum above 100 MeV and the other a Gaussian. Two combinations, one 50 percent a detector resolution function and 50 percent a Gaussian with a 1 σ of 6°, the other 60 percent a detector resolution function and 40 percent a Gaussian with a 1 σ of 7°, give nearly equally good fits under the χ^2 test. Relatively small variations from these, such as a 40–60 percent or a 60–40 split from the 6° Gaussian case or any combination with a 5° Gaussian give a χ^2 at least twice as large. Any attempted fit using a single Gaussian produced at χ^2 at least 5 times as large as the best fit using two curves. In terms of galactic structure, this result implies that the origin of the radiation is about equally divided between close (<2 or 3 kpc) and more distant regions, since galactic features beyond about 3 kpc are narrower in b^{II} than the detector angular resolution. Using a detector with angular resolution ~2° above 20 MeV, Samimi, Share, and Kinzer (1974) report that the bulk of the galactic-plane emission appears to lie in a band about 3° wide at these energies.

In Figure 8*b* the distribution in b^{II} for γ-rays with measured energies above 100 MeV and with $90° < l^{\text{II}} < 180°$ and $200° < l^{\text{II}} < 260°$ is shown. This region excludes the large flux from the Vela and Crab

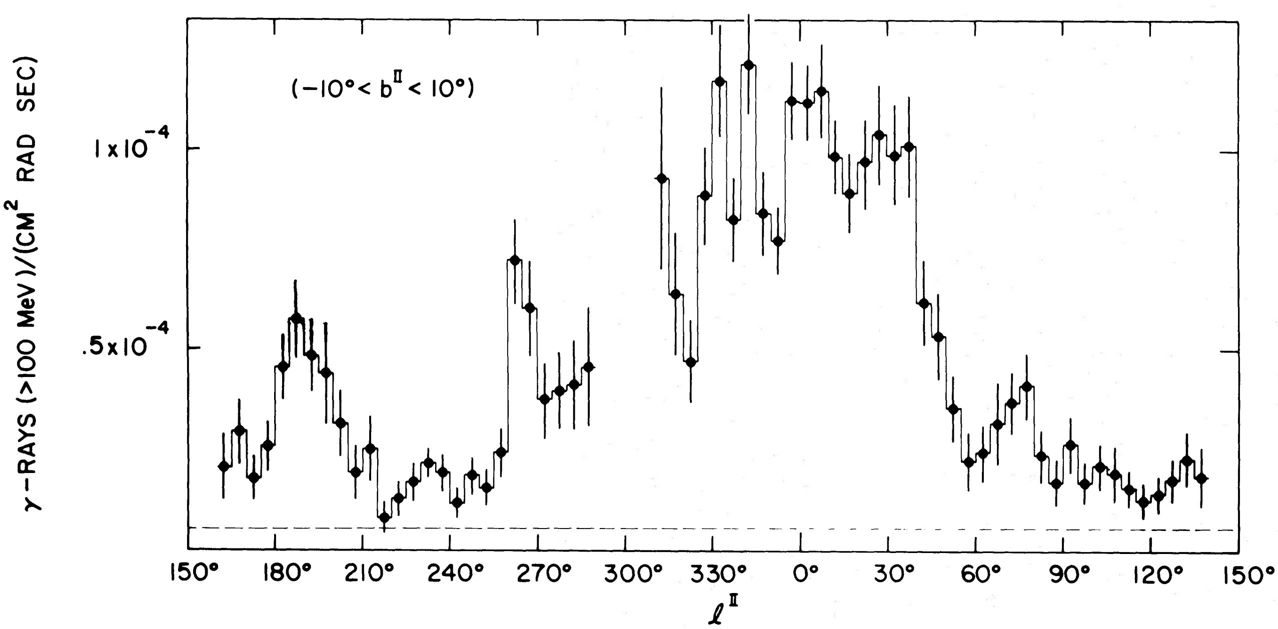

FIG. 7.—Distribution of high-energy (>100 MeV) γ-rays along the galactic plane. The SAS-2 data are summed from $b^{\text{II}} = -10°$ to $b^{\text{II}} = +10°$. The diffuse background level is shown by a dashed line. The error bars reflect calibration, energy resolution, and statistical uncertainties.

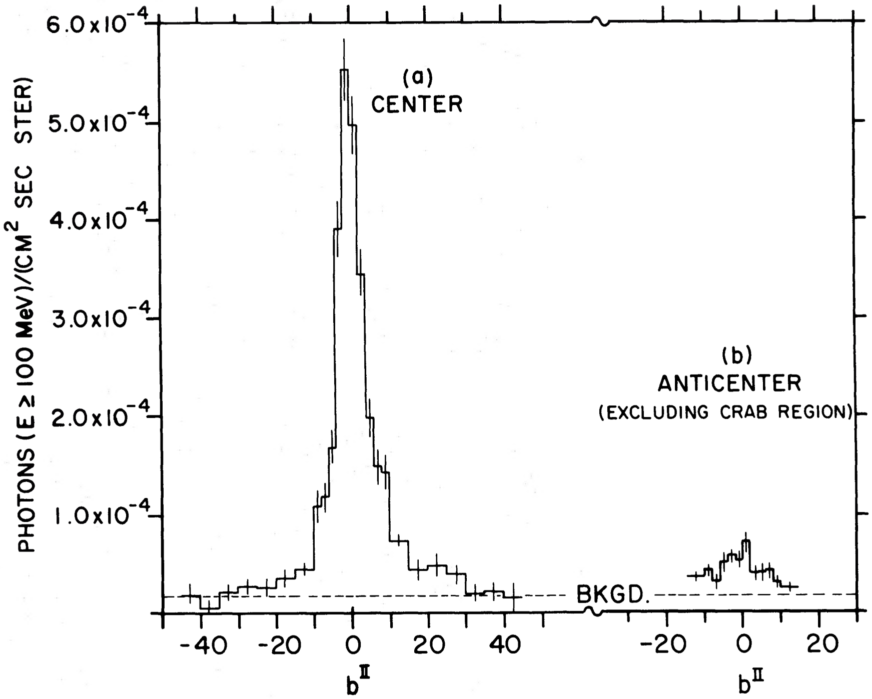

FIG. 8.—(*a*) Distribution of high-energy (> 100 MeV) γ-rays summed from $l^{II} = 330°$ to $l^{II} = 30°$ as a function of b^{II}. The diffuse background is indicated by a dashed line. (*b*) Distribution of high energy (> 100 MeV) γ-rays summed from $90° < l^{II} < 170°$ and $200° < l^{II} < 260°$, where data exist, as a function of b^{II}. The diffuse background is indicated by a dashed line.

regions. The lack of a narrow peak in this case suggests that most of this radiation is coming from relatively close regions, as expected from the location of the solar system in the Galaxy. The other distinctive aspect of Figure 8 is the very much greater intensity of the galactic radiation in the $330° < l^{II} < 30°$ region, which was also shown in Figure 7.

In Figure 8, also note that, whereas the 100-MeV γ-radiation approaches the diffuse background level by about $|b^{II}| = 15°$ on the negative b^{II} side in the center regions, it remains relatively high to $b^{II} = +30°$ on the positive side of the ($330° < l^{II} < 30°$) region. A lesser enhancement is observed on the negative side of the interval $160° < l^{II} < 200°$. When examined more closely, there is a hint that these regions correlate with Goud's Belt, but the limited statistics make it difficult to assign specific locations to the excesses.

A figure similar to Figure 7 is obtained when the galactic plane radiation above 100 MeV is plotted in 5° l^{II} intervals, but summed only in the interval ($-4° < b^{II} < 4°$). The principal difference, besides slightly larger uncertainties in individual points, is a larger ratio for the radiation from ($325° < l^{II} < 40°$) to that from ($90° < l^{II} < 180°$) or from ($200° < l^{II} < 260°$), as expected since the narrower, more distant features are enhanced. The ($75° < l^{II} < 80°$) peak also is somewhat more significant.

Returning to Figure 7, the entire excess in the region 260° to 270° lies south of the galactic plane and can be attributed to the region around Vela X, centered about $b^{II} = -3°$, $l^{II} = 265°$. The high-energy γ-ray excess was reported previously (Thompson *et al.* 1974) and will be discussed further in § III*d*. The excess in the region $180° < l^{II} < 190°$ can be attributed to the Crab Nebula. The remainder of the excess from about 185° to 200° in l^{II} is a few degrees above the galactic plane. The enhanced region starting presumably before $l^{II} = 310°$ (there is a gap in data from 290° to 310°) and extending to 50° to 55° corresponds roughly to the angular extent of the strong inner galactic arms. The possible theoretical explanation for the high-energy γ-radiation from the galactic plane will be pursued in detail in § III*a*(ii), along with a more detailed discussion of the relationship of the galactic structure to the γ-radiation.

The energy spectrum of the radiation for the region $330° < l^{II} < 30°$ is shown in Figure 9 after subtracting the diffuse background, which is small—between 6 and 7 percent above 100 MeV. The errors shown result primarily from calibration and energy resolution uncertainties, since over 2400 γ-rays are included in the analysis. After subtracting the diffuse background, the energy spectrum from the rest of the galactic plane is similar, or possibly slightly harder. The γ-radiation from the Vela region has an energy spectrum indistinguishable from the rest of the plane.

The average intensity above 100 MeV is seen in Figure 9 to be $(0.96 \pm 0.14) \times 10^{-4}$ γ-rays cm^{-2} rad^{-1} s^{-1} for the interval ($330° < l^{II} < 30°$, $-10° < b^{II} < 10°$) after the diffuse background, equivalent to $(0.066 \pm 0.009) \times 10^{-4}$ is subtracted. This energy spectrum is consistent with a two component model

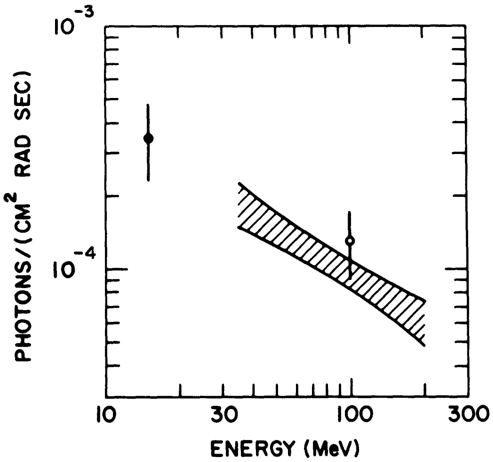

FIG. 9.—Energy spectrum for γ-rays from the region ($-10° < b^{II} < +10°$, $330° < l^{II} < 30°$). The shaded region shows the spectrum measured by SAS-2, unfolded from the detector response, together with its uncertainty. Data shown for comparison and from Kraushaar *et al.* (1972) (*open circle*) and Share, Kinzer, and Seeman (1974*a*) (*solid circle*). Other results and upper limits are discussed in the text.

consisting of a $\pi°$ decay type spectrum and a differential power law of the form $dJ/dE = AE^{-2.0}$, within the limits shown in Figure 9.

Other results shown in Figure 9 include the results of Kraushaar *et al.* (1972) and Share, Kinzer, and Seeman (1974*a*). The high-altitude balloon experiments all have the difficult problem of the atmospheric background. Nonetheless, data from these at high energies (≥ 100 MeV), some positive results and other upper limits (Frye *et al.* 1971, 1974; Bennett *et al.* 1972; Fichtel *et al.* 1972; Dahlbacka, Freier, and Waddington 1973; Sood *et al.* 1974), agree with the results shown in Figure 9 within rather large uncertainties, except Frye *et al.* (1974), who report values well below those shown.

ii) *Discussion*

The energetic galactic γ-rays are generally thought to result primarily from the interaction of cosmic rays with interstellar matter. This concept will be examined here in terms of some of the models that have been proposed after a brief review of the parts of the basic calculation of particular importance here.

The number and energy spectrum of the γ-rays produced by cosmic rays interacting with interstellar matter have been calculated in detail for the case of the cosmic radiation in interstellar space by several authors—e.g., Stecker (1973) and Cavallo and Gould (1971) for the proton interactions and Bussard (1974) for the electron interactions. The flux of γ-rays with energies greater than E at a distance r is given by the expression

$$\Phi(E) = \tfrac{1}{4}\pi \int S(E)g(r, d\theta, d\phi)n(r, d\theta, d\phi)dr(\sin\theta d\theta d\phi)\,, \quad (2)$$

where S is the number of γ-rays produced per second on the average for one interstellar nucleon plus electron and a cosmic-ray density and spectrum equal to that near the Earth, n is the interstellar number density, and g has been introduced here to represent the ratio of the cosmic-ray density to that in the vicinity of the solar system. The interstellar nucleon component is primarily of importance for cosmic-ray nuclear particles; and the electron, for cosmic-ray electrons. However, assuming the Galaxy to be neutrally charged on the average, the net effect of the two phenomena can be treated together in one equation such as equation (2).

The principal contribution to the high-energy ($\geq 10^2$ MeV) γ-radiation from the cosmic-ray nuclear interactions with interstellar matter comes in the cosmic-ray energy range from a few tenths of a GeV to a few tens of GeV. Below that energy range the parent π^0 mesons leading to γ-rays are not produced, and at higher energies the contribution is very small because the cosmic-ray energy spectrum is decreasing much faster with energy ($\sim E^{-5/2}$) than the pion production is increasing ($\sim E^{1/4}$). The contribution from the cosmic-ray electrons becomes important primarily in the lower part of the γ-ray energy range being considered here. The overall source function $S(E)$ has the value 1.6×10^{-25} s^{-1} above 100 MeV, using for the nucleonic component the value given by Stecker (1973) and for the electrons that given by Bussard (1974), based on the cross sections of Koch and Motz (1959) and the electron spectrum deduced by Goldstein, Ramaty, and Fisk (1970).

Compton and synchrotron radiation are generally not thought to be dominant in the production of high-energy γ-rays. Compton radiation could originate either from cosmic-ray electrons interacting with starlight or the blackbody radiation; however, neither should make a significant contribution unless either the cosmic-ray electron density is proportionally much larger elsewhere in the Galaxy or starlight should increase dramatically (by almost two orders of magnitude) toward the galactic center. As a consequence, the calculated longitudinal distribution in pure Compton radiation models generally peaks much too sharply at $l^{II} = 0°$ (e.g., Cowsik 1974) to be consistent with the observations reported here. Synchrotron radiation will also not be important unless again the field strength increases very rapidly toward the inner part of the Galaxy.

In the first attempts to compare the observed high-energy γ-ray intensity with calculated values, it was assumed (e.g., Kraushaar *et al.* 1972) that the cosmic-ray density was uniform throughout the Galaxy so that g could be taken outside the integral in equation (2) and was usually set equal to 1. Using the 21-cm data to estimate columnar hydrogen density, Kraushaar *et al.* (1972) showed that whereas the calculated intensity was fairly close to that expected in the anticenter direction when the expected intensity was integrated over the solid angle of the detector (which had a Gaussian angular sensitivity with a 1 σ of about 15°), the observed intensity in the galactic center region was about 4 times the calculated value. Thus, the galactic longitudinal dependence was inconsistent with this model, and it could not be brought into agreement by assuming a uniformly higher value of the cosmic-ray density or by assuming that the total matter density was uniformly much higher because a significant portion of the interstellar hydrogen was in molecular form, for example.

More recently, Strong, Wdowczyk, and Wolfendale (1973) assumed that the cosmic-ray density shows a smooth increase toward the galactic center in accordance with an expression of Thielheim and Langhoff (1968) for the mean magnetic field or the square of this field. This work, although not in agreement with present results, was one of the first to break with the concept of constant cosmic-ray density. Schlickeiser and Thielheim (1974) have extended this approach by using an analytic formula for the concentration of magnetic fields, cosmic rays, and matter in galactic spiral arms.

Stecker *et al.* (1974) proposed that the galactic cosmic-ray intensity varies with the radial distance from the galactic center and is about an order of magnitude higher than the local value in a toroidal region between 4 and 5 kpc. They further suggest that this enhancement can be plausibly accounted for by Fermi acceleration caused by a hydrodynamic shock driven by the expanding gas in the "4 kpc" arm and invoked in some versions of galactic structure theory. This theory does provide a possible explanation of the general enhancement in the central region as shown, but not some of the other features now beginning to appear. There is, of course, also the question of whether or not the Fermi acceleration exists. If it does, then, clearly, the accelerated cosmic rays could play an important role.

In pursuing the problem of galactic γ-radiation, it is important to realize that the full-width angular resolution of the high-energy γ-ray detectors flown thus far has been either several degrees, in the case of SAS-2, or about 24° in the case of OSO-3. Thus, the observed intensity of a feature with a thickness comparable to the disk of the Galaxy will decrease approximately as the reciprocal of the distance once it is more than 2 kpc away from SAS-2 (and closer for OSO-3), and faster if it is also small in extent within the plane. Hence, more distant regions of the Galaxy would have to be substantially more intense than local ones to explain an observed intensity of γ-rays in any given direction with the present instruments. This consideration, together with the geometrical distribution of the intense high-energy γ-radiation, particularly the broad distribution of the γ-radiation in galactic longitude over 70° to 90° in the central region of the Galaxy, suggested to Kniffen *et al.* (1973) that the source of the enhancement is possibly predominantly diffuse radiation from the spiral arm segments closest to the Sun in the direction of the galactic center.

Bignami and Fichtel (1974) proceeded further and proposed that in general the cosmic rays are enhanced where the matter is greatest—namely, in the arm segments. This hypothesis is supported by the following considerations: First, it is assumed that the cosmic rays and magnetic fields are galactic and not universal. Then, as shown by Bierman and Davis (1960) and Parker (1966) in more detail, the magnetic fields and cosmic rays can only be contained by the weight of the gas through which the magnetic fields penetrate; hence, they are tied to the matter. The galactic cosmic-ray energy density cannot substantially exceed that of the magnetic fields, or the cosmic-ray pressure would push a bulge into the fields, ultimately allowing the cosmic rays to escape. The local energy density of the cosmic rays is about the same as the estimated energy density of the average magnetic fields and the kinetic motion of matter. Together the total pressure of these three effects is estimated to be approximately equal to the maximum that the gravitational attraction can hold in equilibrium. This suggests that the cosmic-ray density may generally be as large as would be expected under quasi-equilibrium conditions. This concept is also given some theoretical support by the calculated slow diffusion rate of cosmic rays (e.g., Parker 1969; Lee 1972; Wentzel 1974) in the magnetic fields of the Galaxy based on the cosmic-ray lifetime and the small cosmic-ray anisotropy and the likely high production rate of cosmic rays, which together suggest that in general the cosmic rays should be plentiful in a given region and will not move quickly to less dense regions. Therefore, it was assumed that the energy density of the cosmic rays is larger where the matter density is larger. As a trial assumption, Bignami and Fichtel (1974) let the cosmic-ray density be proportional to the matter density on the scale of galactic arms. The fluctuations in matter density are then quite important in determining the expected gamma-ray intensity calculated by equation (2) since the γ-radiation becomes proportional to n^2.

The spatial distribution of interstellar matter has generally been estimated from 21-cm radio data—which, however, indicate only atomic hydrogen densities and do not include the ionized and molecular hydrogen. There are in addition some problems associated with the direct interpretation of the 21-cm data as discussed, for example, by Simonson (1970). Relying on measurements from external galaxies and on the density-wave theory for the spiral pattern (e.g., Roberts and Yuan 1970), Bignami and Fichtel (1974) assume that the inner galactic arms had an arm-to-interarm density ratio of 5 to 1. With this assumption, the center-to-anticenter ratio and the absolute intensity can be explained, as well as the distribution within the $310° < l^{\mathrm{II}} < 50°$ interval in the general way permitted by a cylindrical model approximation. With the higher molecular density now thought to exist in the inner part of the Galaxy, the arm-to-interarm ratio could be reduced substantially and still provide agreement with the experimental results.

In this model, the Sagittarius arm makes a major contribution, and it is close enough in the $l^{\mathrm{II}} = 0°$ direction that its width in b^{II} is greater than the detector resolution. Figure 8, as noted earlier, clearly shows a distribution of at least two components.

Recently Scoville and Solomon (1975) have used 2.6-mm radio measurements they have made of the CO emission line to estimate the molecular hydrogen density distribution in the Galaxy based on the hypothesis (Scoville and Solomon 1974; Goldreich and Kwan 1974) that the most important source of CO excitation in galactic clouds is the collision of CO with H_2. Using the cylindrically symmetric Schmidt model, they concluded that the molecular hydrogen density is relatively large, between 1 and 5 molecules cm^{-3}, in the region from 4 to 7 kpc from the galactic center, with the maximum density between 5 and 6 kpc. Since this mass density range is from 1 to 10 times the atomic hydrogen density assumed in most previous work, its contribution to the γ-radiation could be substantial if the higher side of the range is correct. Cowan, Kafatos, and Rose (1974) have noted the important implication of a higher molecular hydrogen density, and Solomon and Stecker (1974) have suggested that this ring could be the major source of the observed γ-radiation.

Returning to Figure 7, the sharp decrease between $l^{II} = 50°$ and 55° is consistent with the tangent to the Sagittarius arm as shown in Figure 10 (Simonson 1973). The valley from 50° to 70° is consistent with the lack of features in that direction and the increase in Cygnus from 70° to 80° is consistent with the direction of the Orion arm.

In addition to the central arms making a strong general contribution, actual peaks in the γ-radiation are expected at directions along the galactic arms. Maxima would then be expected between 310° and 315°, 330° and 335°, and 340° and 345° in l^{II} corresponding to the Scutum, Norma, and 4-kpc arms. Peaks in these regions are indeed seen in Figure 7. Whereas any one peak may not be considered statistically significant (the error bars in Fig. 7 included more than the statistical uncertainty), the fact that all three peaks are observed is clearly a striking feature. On the other side of the plane the arms are closer to the Sun and not as clearly separated; however, the 4-kpc and Scutum arm tangents fall in the 20°–40° interval and only Sagittarius of the strong inner arms is left beyond 40°, consistent with the observations. There also appears to be a contribution from the galactic center itself, or other sources in that direction.

These results suggest that all the principal galactic-arm segments between the solar system and the galactic center are playing a significant role in the origin of the high-energy γ-radiation, and, although the 4-kpc "ring" may be making an important contribution, it is not necessarily dominating the γ-radiation observed at the Earth. The combination of the galactic longitudinal and latitudinal distributions seem to support well the concept of cosmic rays and matter being concentrated into arm segments, although the determination of the molecular hydrogen is most important to a complete understanding of this situation.

Point or localized sources of γ-rays may be making a contribution to the galactic intensity in addition to those already mentioned. It will most probably not be

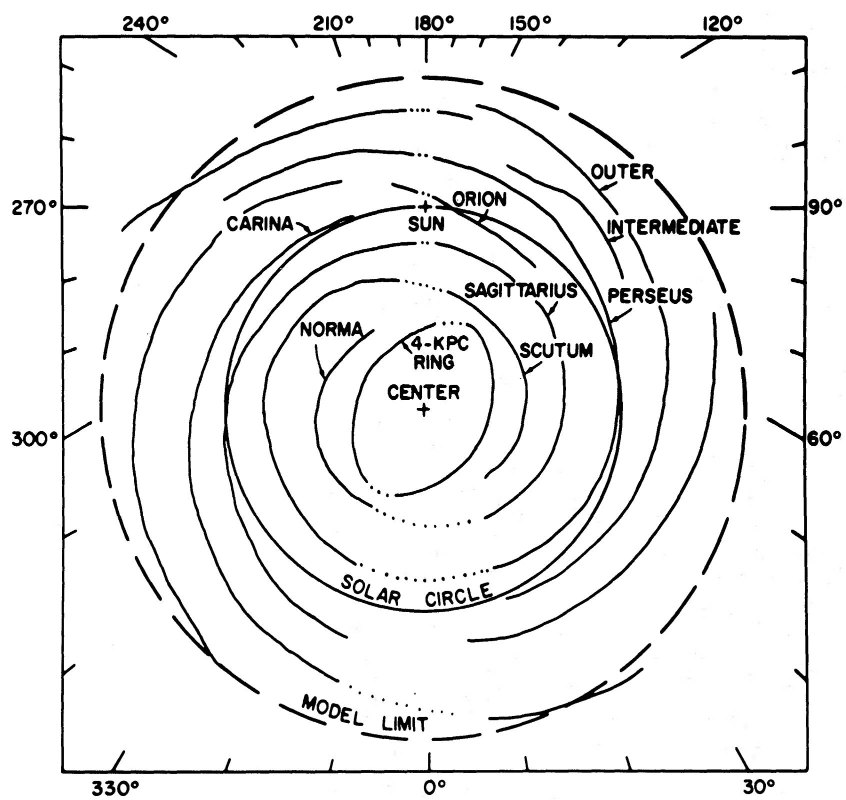

FIG. 10.—A smoothed spatial diagram of the locations of the maxima of the matter density deduced from 21-cm H I line measurements and the density wave theory (Simonson 1973).

possible to determine if they are a significant contribution until γ-ray telescopes with better angular accuracy than SAS-2 are flown. It has been suggested that the steep spectra of most of the X-ray sources speak against many significant γ-ray point sources in the Galaxy, but, since γ-ray production mechanisms are very different, the γ-ray sky probably looks very different from the X-ray sky, just as the X-ray sky looks very different from the optical sky. Hence, the question must remain open.

At present, the high-energy galactic γ-radiation seems adequately explained as resulting primarily from cosmic-ray interactions with matter, and this explanation is supported not only by the magnitude of the radiation but also by its galactic longitudinal and latitudinal distributions.

b) Diffuse Radiation

i) *Experimental Results*

One of the areas of interest for the SAS-2 experiment is the study of a possible diffuse component of the celestial γ-ray intensity, especially since such a diffuse intensity would probably originate outside the Galaxy. Measurements of this radiation could therefore provide information and constraints on theories involving extragalactic cosmic-ray and matter densities, both at the present and in the cosmological past, and on antimatter distributions such as those proposed in the baryon-symmetric big-bang cosmology.

The OSO-3 γ-ray experiment of Kraushaar *et al.* (1972) observed an apparently diffuse intensity for regions of the sky which did not include the galactic plane. An integral value of $(3.0 \pm 0.9) \times 10^{-5}$ photons cm^{-2} s^{-1} sr^{-1} was obtained for the intensity above 100 MeV, but essentially no energy spectral information was available. In a previous paper, preliminary results from SAS-2 showed that the diffuse intensity had a steep energy spectrum (Fichtel, Hartman, and Kniffen 1973*b*).

SAS-2 data from six regions of the sky away from the galactic plane have now been examined. A uniform, apparently diffuse, intensity has been measured for that portion of these regions with $|b^{\rm II}| > 30°$. The detector pointing directions were ($l^{\rm II} = 0°, b^{\rm II} = +25°$), ($l^{\rm II} = 0°, b^{\rm II} = +58°$), ($l^{\rm II} = 19°, b^{\rm II} = -23°$), ($l^{\rm II} = 190°, b^{\rm II} = -30°$), ($l^{\rm II} = 285°, b^{\rm II} = +75°$), and ($l^{\rm II} = 300°, b^{\rm II} = -45°$). Only γ-rays arriving within 25° of the detector pointing direction were accepted for analysis.

The data with $|b^{\rm II}| > 30°$ from these regions show a γ-ray intensity which is uniform in both intensity and energy spectrum, within statistics. Data from these areas have been combined into the diffuse energy spectrum shown in Figure 11. This differential energy spectrum is steeper than any other spectra observed on SAS-2 or the earlier balloon work of this group with a similar detector (e.g. Fichtel, Kniffen, and Ögelman 1969; Fichtel *et al.* 1972). The shaded area represents the diffuse spectrum seen by SAS-2, unfolded from the detector response, along with the uncertainty in the measurement. Representing the energy spectrum by a power law of the form $dJ/dE = AE^{-\alpha}$ photons cm^{-2} s^{-1} sr^{-1} MeV^{-1} over the SAS-2 energy range of 35 to 200 MeV, α is found to be 2.4 ± 0.2. The integral flux above 100 MeV is measured to be $(1.93 \pm 0.26) \times 10^{-5}$ photons cm^{-2} sr^{-1} s^{-1}, wherein the error includes statistical, calibration, and energy resolution uncertainties, but not any effect resulting from possible region-to-region variations.

The only noncelestial background contribution to this γ-ray component is that due to interactions of cosmic-ray particles within the material surrounding the detector, principally the 0.15 g cm^{-2} thick thermal blanket. Such interactions would have to produce a γ-ray in the field of view of the detector without leaving a charged particle with energy and direction such as to trigger the anticoincidence system. Monte Carlo calculations indicate that this contribution is well over an order of magnitude below the measured diffuse intensity even at the highest energies considered by SAS-2. Additional evidence against a significant background for this component is the observed spectral distribution which is totally different from the spectrum expected from cosmic-ray interactions in the detector material.

The integral flux value reported here lies somewhat below the OSO-3 result (Kraushaar *et al.* 1972), but the two values agree within errors, and the OSO-3 result probably contains a small local galactic component since considerable data with $|b^{\rm II}| < 30°$ (and even some with $|b^{\rm II}| < 15°$) were included as a result of the rather wide acceptance angle of the OSO-3 detector (FWHM $\approx 24°$). The SAS-2 results are seen to be in agreement with the upper limits set by other experiments (Bratolyubova-Tsulukidze *et al.* 1971; Hopper *et al.* 1973; Share, Kinzer, and Seeman 1974*b*) but disagree with the observation of Herterich *et al.* (1973).

Taken as a whole, the measurements of the diffuse γ-ray spectrum do not present a simple picture. The line labeled B in Figure 11 is a plot of the function $dJ/dE = 0.011E^{-2.3}$ in units of photons cm^{-2} s^{-1} sr^{-1} MeV^{-1} with E expressed in MeV. This line was chosen to pass through both the SAS-2 data and the <1 MeV γ-ray data. This curve is also consistent with the high energy X-ray data within uncertainties (Schwartz and Gursky 1973; Dennis, Suri, and Frost 1973). However, the majority of the data from 1 to 10 MeV seem to lie above and have a flatter spectral shape than this power law would indicate, implying first a decrease and then an increase in spectral slope. The intensity in the 5–40 MeV energy range is quite uncertain at this time.

ii) *Discussion*

Until more regions of the sky are included in the SAS-2 data, no statement is possible concerning the degree of uniformity of the radiation away from the galactic plane. The steep spectrum observed by SAS-2 away from the galactic plane lends weight to the hypothesis that this radiation is not simply a combination of many sources with the type of γ-ray source mechanism seen in our own Galaxy.

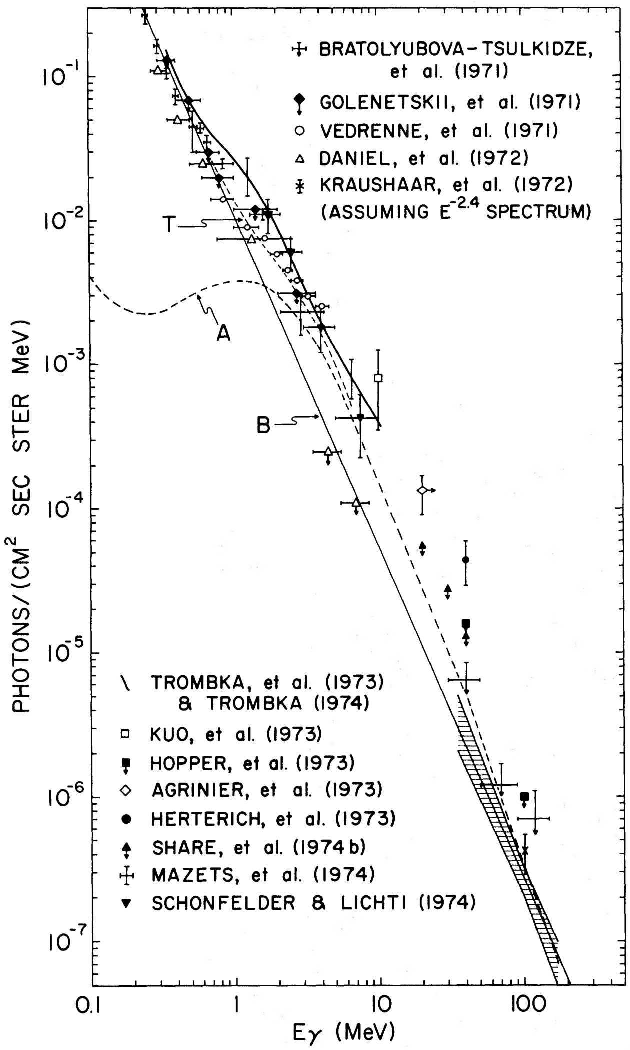

FIG. 11.—Diffuse celestial radiation observed by several experiments. The shaded area represents the SAS-2 data unfolded from the detector response, together with its uncertainty. The symbols for other results are explained in the Figure. The line B is the function $0.011E^{-2.3}$ photons/(cm^2 s sr MeV), as discussed in the text. The dashed lines A and T represent the calculations of Stecker *et al.* (1971) based on the matter-antimatter annihilation of the baryon-symmetric cosmology (A) and the annihilation curve plus a low energy power-law component (T). The curves have been normalized to reflect recent measurements. The results of Vedrenne *et al.* (1971) and Daniel *et al.* (1972) are shown without error bars. The estimated uncertainty in these points is 50%.

Under the assumption that the regions of the sky already examined are representative of a diffuse celestial intensity, the theoretical implications can be considered. Whenever cosmic rays and matter coexist, γ-rays are produced by nuclear collisions; and, once produced, γ-rays in the energy range viewed by SAS-2 suffer very little attenuation in space. These facts make possible the use of the SAS-2 observations to set limits on the extent of the region in which cosmic rays can exist at a level comparable to that observed at Earth. Several assumptions must be made in order to set such limits, the first of which is the choice between an open and closed universe. Under the assumption of a closed universe, a reasonable estimate for the intergalactic matter density is about 10^{-5} protons cm^{-3}. With this matter density, cosmic rays could not exist at the local level beyond a radius of about 50 Mpc, since the resultant γ-ray intensity above 150 MeV as calculated from equation (2) would then be higher than what has been observed by SAS-2. Thus, a cosmic-ray density equal to that near the Earth cannot pervade a closed universe, but the possibility that cosmic rays at the local density exist throughout our local supercluster of galaxies cannot be eliminated. The open universe permits much lower intergalactic densities, but it is then necessary to consider specific cosmological models because contributions from large distances and hence high redshifts are involved. These considerations will be treated shortly, together with other possible origins for the diffuse radiation.

The list of candidate models to explain the diffuse radiation is lengthy, and an analysis of many of these would be beyond the scope of this paper. Nevertheless, from the point of view of the SAS-2 measurements, several of these models deserve attention. The basic features of the diffuse γ-ray spectrum which any model must explain are the apparent spectral flattening in the 1 to 10 MeV energy range and the flux and steep spectrum above 30 MeV.

The diffuse γ-rays may originate from diffuse electrons interacting with matter, photons, or magnetic fields. Bremsstrahlung seems unlikely, since, in an energy region 1–10 MeV, where an increased slope would be expected due to an increasing rate of energy loss, the opposite is observed. For both synchrotron and Compton radiation, the observed photon spectrum would imply a similarly shaped parent electron spectrum which would have even sharper spectral features. Further, for all three cases, the observed intensity seems high to be consistent with reasonable estimates of the intergalactic parameters.

Of the pure γ-ray cosmological hypotheses, there are at least three that seem to be possible candidates. They are particle-antiparticle annihilation in the baryon-symmetric big-bang model, the cosmic-ray–intergalactic-matter interaction model, and the cosmic-ray–blackbody interaction model. In all theories, the resulting γ-ray spectrum is redshifted substantially by the expansion of the universe.

Harrison (1967) was one of the first to propose a model of the big-bang theory of cosmology with the principle of baryon symmetry. Omnès (1969), following Gamow (1948), considered a big-bang model in which the universe is initially at a very high temperature and density, and then showed that, if the universe is baryon-symmetric, a separation of matter and antimatter occurs at $T > 30$ MeV. The initial phase separation of matter and antimatter leads ultimately to regions of pure matter and pure antimatter of the size of galaxy clusters. Stecker, Morgan, and Bredekamp (1971) have predicted the γ-ray spectrum which would be expected from π^0 decay arising from an annihilation of nucleons and antinucleons at the boundaries of such clusters from the beginning of their existence to the present. This spectrum is shown in Figure 11.

In an expanding model of the universe, the density of matter is much greater in the cosmological past than in the present; and if cosmic rays are present, they interact with this matter, leading to γ-rays whose energies are once again redshifted as observed at the present time. One curve developed by Stecker (1969) involving redshifts up to about 100 is essentially indistinguishable from curve A in Figure 11 in the energy range for which data exist and is not shown for this reason. This model does imply, however, an implausibly high cosmic-ray energy density at early times in the universe.

A third cosmological model involves cosmic-ray interactions with the blackbody radiation at an early point in cosmological time. Wolfendale (1974) has shown that this theory is also a possibility.

For the present the origin and nature of the diffuse γ-ray intensity must remain an open question. In particular, both the large- and small-scale uniformity of the diffuse radiation need to be established more firmly, together with improved determination of the energy spectrum at all energies.

c) *Localized Sources*

Gamma-ray astronomy has been limited in its search for localized sources by the lack of good angular resolution, low counting statistics, and the atmospheric background in the case of balloon experiments. The SAS-2 experiment provides a sensitivity for the detection of discrete sources over an order of magnitude better than that of previous measurements. The marked improvement results from the combined factors of increased sensitivity, better angular resolution, and reduced background. Substantial improvements are still possible over the SAS-2 experiment for future γ-ray telescopes.

Positive fluxes have already been reported from SAS-2 for the Crab Nebula (Kniffen *et al.* 1974) and the Vela region (Thompson *et al.* 1974). The Crab emission, observed during the period 1972 December 14–21, is characterized by a strong pulsed component from NP 0532 with both the pulsed and unpulsed components consistent with a power-law extension of observations at lower energies extending to at least a GeV. The total flux above 100 MeV is observed to be $(3.2 \pm 0.9) \times 10^{-6}$ photons cm^{-2} s^{-1}. The Vela emission above 100 MeV is observed to be $(5.0 \pm 1.2) \times 10^{-6}$ photons cm^{-2} s^{-1}, and above 35 MeV it is $(1.1 \pm 0.3) \times 10^{-5}$ photons cm^{-2} s^{-1}. Thompson *et al.* (1974) have pointed out the possible association of this excess emission with the Vela supernova remnant. Approximately 6×10^{50} ergs of cosmic rays from the supernova would be contained in the remnant, if the possibility that a portion of the excess may be due to galactic arm segments is excluded.

A comparison has been made of γ-ray arrival times from the Vela region with predicted pulse arrival times for PSR 0833-45. Pulsar data at 2388 MHz (period, period derivative, and phase) were supplied by Reichley (1974) for the week during which the SAS-2 observations were made (1973 February 15–20); the arrival times were corrected by 50.3 ms for dispersion. The γ-ray data were plotted as a function of pulse phase, using the same program previously applied to the Crab Nebula data. No enhancement was seen in phase with the radio pulse, and the upper limit for pulsed γ-rays above 35 MeV in phase with the radio data is 2.1×10^{-6} cm^{-2} s^{-1}. This upper limit corresponds to a value of 1.1×10^{-6} MeV cm^{-2} s^{-1} MeV^{-1}, averaged from 35 to 100 MeV, which seems inconsistent with a power-law extension to higher energies of the recently reported positive pulsed flux at 10–30 MeV of 1.5×10^{-5} MeV cm^{-2} s^{-1} MeV^{-1} (Albats *et al.* 1974). The γ-ray data do show a small peak, following the radio pulse by 11 ms. The probability of such a peak appearing by chance in one of the 33 bins used is about 6 percent, and a positive result is not claimed here. Based on this peak, the upper limit for a pulsed γ-ray flux above 35 MeV from PSR 0833-45, at the radio period, would be 5.1×10^{-6} cm^{-2} s^{-1}.

In addition to these two established high-energy γ-ray sources, the SAS-2 data show other enhancements and provide upper limits on other possible sources. As mentioned in § III*a*, two general regions with $15° < |b^{\mathrm{II}}| < 30°$ along the galactic plane show excesses. The SAS-2 detector also saw an apparent excess of high-energy radiation a few degrees above the galactic plane from about $l^{\mathrm{II}} = 185°$ to $l^{\mathrm{II}} = 200°$, which is too broad to be consistent with a single point source. One object of interest in that region is IC 443 ($l^{\mathrm{II}} = 189°$, $b^{\mathrm{II}} = +3°$), a rather old (~60,000 yr) supernova remnant, the distance to which has been evaluated to be about 1.5 kpc. The shell of this object shows optical and radio evidence of interactions with the adjacent H II region Sh 249 ($l^{\mathrm{II}} = 191°$, $b^{\mathrm{II}} = +4°$) and a system of H I clouds, the density of which has been estimated to be about 10 to 20 atoms cm^{-3} (Akabane 1966; Duin, Strom, and Van der Laan 1973). Recent observations have shown that IC 443 is an X-ray emitter (Winkler and Clark 1974).

In the Cygnus region, the enhanced interval from 70° to 80° in galactic longitude has already been mentioned in § III*a* to coincide with the long line-of-sight path length along the Orion arm. It is worth noting, on the other hand, that the Ilovaisky and Lequeux (1972) catalog of supernova remnants lists nine such objects with $0° < b^{\mathrm{II}} < 6°$ and $74° < l^{\mathrm{II}} < 83°$, of which two have distance estimates less than 2 kpc. An additional remnant in this general region is the Cygnus Loop, which is south of the plane.

Table 1 presents significant new upper limits on objects of interest for which no evidence of a positive γ-ray flux is obtained with SAS-2. A 95 percent confidence upper limit of 9.5×10^{-7} cm^{-2} s^{-1} is obtained for >100 MeV γ-ray emission from Sco X-1, the most intense X-ray source. An upper limit of 1.5×10^{-6} cm^{-2} s^{-1} is obtained for the dark clouds near ρ Oph and in Corona Austrina, suggested by Black and Fazio (1973) as possible origins for the γ-ray excesses reported for the directions $l^{\mathrm{II}} \approx 352°$, $b^{\mathrm{II}} \approx 16°$ (Dahlbacka *et al.* 1973) and $l^{\mathrm{II}} \approx 0°$, $b^{\mathrm{II}} \approx -19°$ (Frye *et al.* 1969; Frye *et al.* 1971). The upper limits obtained with SAS-2 fall over an order of magnitude below the reported fluxes but do not conflict with the theoretical prediction.

Limits (>100 MeV) for other previously reported γ-ray sources within the analyzed regions include 1.2×10^{-6} cm^{-2} s^{-1} for the region $l^{\mathrm{II}} = 340°.7$, $b^{\mathrm{II}} = 30°.3$ (Frye *et al.* 1971), and 2.0×10^{-6} cm^{-2} s^{-1} for $l^{\mathrm{II}} = 163°.8$, $b^{\mathrm{II}} = -9°.5$ (Frye 1972). These again lie at least an order of magnitude below the quoted fluxes. A limit of 2.5×10^{-6} cm^{-2} s^{-1} is obtained for 3C 120, over two orders of magnitude below the flux observed by Volobuyev *et al.* (1971) from this general direction.

IV. SUMMARY

The results from the Second Small Astronomy Satellite γ-ray experiment reported here have revealed

TABLE 1

SAS-2 Localized Source Limits (>100 MeV)
(95 percent confidence)

Object	Periods of Observation*	l^{II} (Degrees)	b^{II} (Degrees)	Flux Limit (10^{-6} photons cm^{-2} s^{-1})
Galaxies:				
Large Magellanic Cloud	12	280	−33	2.4
Small Magellanic Cloud	12	303	−45	1.0
M31	17	121	−21	1.4
M87	9	283.6	+74.5	1.0
Supernova remnants:				
Lupus Loop	1	330.1	+15.1	2.4
Monoceros Nebula	8	205.5	+ 0.2	4.4
Cas A	16, 17	111.7	− 2.1	1.1
Cygnus Loop	15	74.0	− 8.6	1.4
HB 21	16	89.1	+ 4.7	1.2
CTA 1	17	119.5	+10.0	1.1
Tycho's SNR (3C 10)	17	120.4	+ 1.4	1.1
X-ray sources:				
Sco X-1 (3U 1617−15)	7	359.1	+23.8	0.95
Cyg X-1 (3U 1956+31)	15	71.3	+ 3.1	2.7
Cyg X-2 (3U 2142+38)	16	87.3	−11.3	1.2
GX 5−1 (3U 1758−25)	2, 10	5.0	− 1.0	2.9
GX 1+4 (3U 1728−24)	2, 10	1.4	+ 3.9	4.0
GX 3+1 (3U 1744−26)	2, 10	3.0	+ 1.0	2.8
Other objects:				
ρ Oph	2, 7, 10	353	+17	1.5
Corona Austrina	2, 10	360	−18	1.5
Jupiter	11	19.8	−22.1	0.63

* Periods of Observation: (1) 11/20/72 to 11/27/72; (2) 11/28/72 to 12/5/72; (7) 1/4/73 to 1/11/73; (8) 1/11/73 to 1/17/73; (9) 1/17/73 to 1/23/73; (10) 1/24/73 to 1/31/73; (12) 2/8/73 to 2/14/73; (5) 3/1/73 to 3/6/73; (16) 3/6/73 to 3/13/73; (17) 3/13/73 to 3/19/73.

a number of aspects of high-energy γ-ray astronomy:

1. The galactic γ-radiation, which dominates over the diffuse radiation along the entire galactic plane, is most pronounced in a region from $l^{\mathrm{II}} = 335°$ to $l^{\mathrm{II}} = 40°$.

2. When examined in detail, the longitudinal and latitudinal distribution seem generally correlated with galactic structural features, and particularly with arm segments.

3. On the basis primarily of its angular distribution and magnitude, the general high-energy γ-radiation from the galactic plane seems to be explained best as resulting primarily from cosmic-ray interactions with interstellar matter.

4. High-energy γ-ray astronomy then holds the promise of being able to map the high-energy cosmic-ray gas in the Galaxy and study the disturbing effects of the cosmic-ray pressure. Further, since the penetrating power of γ-rays is so high, an unclouded view of the Galaxy should ultimately be possible.

5. From the study of six different regions of the sky with $|b^{\mathrm{II}}| > 30°$, there appears to be a uniform celestial γ-radiation, as suggested by earlier results, especially Kraushaar *et al.* (1972). Over the energy range from about 35 MeV to 170 MeV, the differential energy spectrum has the form

$$\frac{Jd}{dE} = (2.7 \pm 0.5) \times 10^{-7}\left(\frac{E}{100}\right)^{-2.4 \pm 0.2} \quad \gamma\text{-rays cm}^{-2}\,\text{sr}^{-1}\,\text{s}^{-1}\,\text{MeV}^{-1}\,,$$

where E is expressed in MeV.

6. The interpretation of the diffuse flux depends critically on the determination of the flux in the 0.6–35 MeV regions. If the apparent flattening of the spectrum in the 0.6–10 MeV region is verified, the high-energy results presented here, when combined with the lower-energy data, suggest a cosmological origin for this radiation.

7. In addition to the general galactic emission, high-energy γ-radiation was seen from the Crab Nebula (a significant fraction of which is pulsed at the radio pulsar frequency), Vela-X (a supernova remnant whose high-energy γ-radiation possibly provides the first direct experimental evidence associating cosmic rays with supernovae), the general region ($15° < b^{\mathrm{II}} < 30°$, $340° < l^{\mathrm{II}} < 20°$), and a region of few degrees north of the galactic plane around 190° to 195° in l^{II}.

8. Several upper limits to high-energy γ-ray fluxes were also set, including 1.0×10^{-6} for the Small Magellanic Cloud, 9.5×10^{-7} for Sco X-1, 2.5×10^{-6} for 3C 120, 1.0×10^{-6} for M87, and 1.1×10^{-6} for Cas A, in units of photons ($E > 100$ MeV) cm^{-2} s^{-1}.

We wish to express our thanks to the many people who made SAS-2 possible. In particular with regard to the experiment itself, we wish to acknowledge the dedication and expertise of Mr. R. Ross, the detector engineer, Mr. C. Ehrmann, the electronics engineer, Mr. W. Cruickshank, the spark chamber systems mechanical engineer, Mr. M. Calabrese, the structural engineer, Miss A. Fitzkee, the thermal engineer, Mr. S. Derdeyn, the experiment manager, and the many others whose efforts are sincerely appreciated. We also wish to express our gratitude to Mrs. M. Townsend, the SAS Project Manager, and her staff, and to Mr. H. Riblet and his entire team at the Johns Hopkins Applied Physics Laboratory who were responsible for the SAS-2 spacecraft control section. We congratulate the San Marco launch team of Centro Ricerche Aerospaziali for providing SAS-2 with a successful launch. For their efforts in the experimental calibration, we thank the Radiation Physics Branch of the National Bureau of Standards and the Hallendienst staff of the Deutsches Elektronen-Synchrotron. In the data analysis area, we wish particularly to express our appreciation to Mr. P. Bracken, Mrs. R. Marsh, and Mr. P. Yu at Goddard Space Flight Center, and Miss N. Koktuna and Mr. F. Tokdemir at the Middle East Technical University. The METU group wishes to thank the Turkish Scientific and Technical Research Council for their support.

APPENDIX

The formalism for the application of multiple scattering measurements to the determination of electron energies in a multiplate spark chamber has been given by Pinkau (1966, 1968) and Kniffen (1969). From this work it can be easily shown that for a probability distribution $f(x, \phi, y)$ for an electron at depth x in the chamber (Fig. 12), the probability distribution for obtaining successive displacements y, y', and y'' at depths x, $x + m\Delta$, and $x + n\Delta$ in a spark chamber with gap separation Δ (Fig. 13) is given by

$$W(y, y', y'') = \iiint d\phi d\phi' d\phi'' \Delta f(m\Delta, \phi - \phi', y - y' - m\Delta\phi') \times f(n\Delta, \phi' - \phi'', y' - y'' - n\Delta\phi'') \,. \qquad \text{(A1)}$$

Representing $f(x, \phi, y)$ by its Fourier transform

$$f(x, \phi, y) = \frac{1}{(2\pi)^2} \iint_{-\infty}^{\infty} d\eta_1 d\eta_2 F(x, \eta_1, \eta_2) \exp{(i\phi\eta_1 + iy\eta_2)}\,,$$

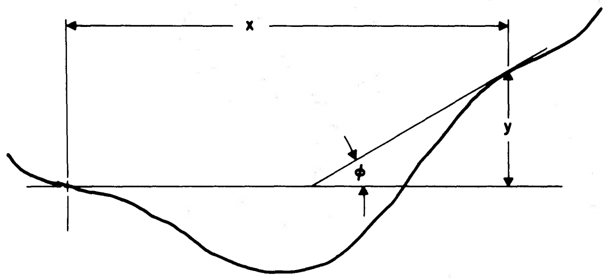

FIG. 12.—Coordinates used in the scattering distribution function

W becomes

$$W(y, y', y'') = \frac{1}{(2\pi)^4} \iiint d\phi d\phi' d\phi'' \iint d\eta_1 d\eta_2 F(m\Delta, \eta_1, \eta_2) \exp\,[i\eta_1(\phi - \phi') + i\eta_2(y - y' - m\Delta\phi')]$$

$$\times \iint d\eta_3 d\eta_4 F(n\Delta, \eta_3, \eta_4) \exp\,[i\eta_3(\phi' - \phi'') + i\eta_4(y' - y'' - n\Delta\phi'')]\,. \tag{A2}$$

Using the relationship $\int_{-\infty}^{\infty} e^{i\eta\phi} d\phi = 2\pi\delta(\eta)$, $W(y, y', y'')$ becomes

$$W(y, y', y'') = \frac{1}{2\pi nm\Delta} \int_{-\infty}^{\infty} d\eta F\left(m\Delta, 0, \frac{\eta}{m\Delta}\right) F\left(n\Delta, \eta, \frac{-\eta}{n\Delta}\right) \exp\left\{\frac{i\eta}{\Delta}\left[\frac{my - (n + m)y' - ny''}{nm}\right]\right\}. \tag{A3}$$

From Moliere scattering theory (Moliere 1955), it can be shown (Pinkau 1966) that the dominant term of the Fourier transform function is given by

$$F(n\Delta, \eta_1, \eta_2) = \exp\,[-J_d^2(u_n\eta_1^2 + v_n\eta_1\eta_2 + w_n\eta_2^2)]\,,$$

with

$$u_n = nd\,, \qquad v_n = n^2 d\Delta\,, \qquad w_n = n\frac{d}{4}\left(\Delta^2 + \frac{d^2}{3}\right) + \frac{(n + 1)n(n - 1)}{3} d\Delta^2\,,$$

where

$$J_d = \frac{1}{X_0} \frac{112}{\log 183Z^{-1/3}} \frac{z^2}{(pv)^2} B_d\,, \frac{1}{B_d} e^{B_d} = \frac{6.68 \times 10^3}{\beta^2} \frac{d}{A} \frac{(Z + 1)Z^{1/3}z^2}{(1 + 3.34\alpha^2)}\,,$$

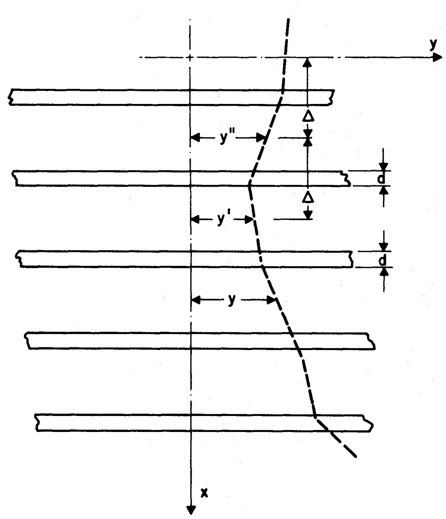

FIG. 13.—Scattering coordinates for the SAS-2 multiplate spark chamber ($d = 0.01$ cm and $\Delta = 1.14$ cm)

$d = d_0/\cos\langle\phi\rangle$, where $\langle\phi\rangle$ is the average angle of the particle trajectory through the scattering plate, d_0 is the plate thickness, X_0 is the radiation length of the scattering material with atomic number Z and mass A, $\alpha = zZ/137\beta$, and z and β are the charge and velocity of the electron. Hence

$$F\left(m\Delta, 0, \frac{\eta}{m\Delta}\right) = \exp\left[\frac{J_d^2}{4}\left(w_m \frac{\eta^2}{m^2\Delta^2}\right)\right]$$

and

$$F\left(n\Delta, \eta, \frac{-\eta}{n\Delta}\right) = \exp\left[\simeq\frac{J_d^2}{4}\left(u_d\eta^2 - v_n\frac{\eta^2}{n\Delta} + w_n\frac{\eta^2}{n^2\Delta^2}\right)\right].$$

Defining $\beta_{mn} = ny - (n+m)y' + my''$, W then becomes

$$W(\beta_{mn}) = \frac{1}{2\pi}\iint_{-\infty}^{\infty} d\eta F(m\Delta, 0, n\eta)F(n\Delta, mn\Delta\eta, -m\eta)\exp(i\eta\beta_{mn})$$
$$= \frac{1}{2\pi}\int_{-\infty}^{\infty} d\eta \exp\left(\simeq\frac{J_d^2}{4}\eta^2\right)(w_{mn}^2 + u_n n^2 m^2\Delta^2 - v_n m^2 n\Delta + w_n n^2)\exp(i\eta\beta_{mn}). \quad \text{(A4)}$$

Defining

$$Q_{mn}^2 = [w_n n^2 + u_n n^2 m^2\Delta^2 - v_n m^2 n\Delta + w_n m^2] = w_m n^2 + w_n m^2,$$

$$W(\beta_{mn}) = \frac{1}{2\pi}\int_{-\infty}^{\infty} d\eta \exp\left[-\frac{J_d^2\eta^2}{4}Q_{mn}^2\right]\exp(i\eta\beta_{mn}) = \frac{2}{J_d Q_{mn}\sqrt{\pi}}\exp\left(\frac{\beta^2}{J_d^2 Q_{mn}^2}\right), \quad \text{(A5)}$$

and hence

$$\langle|\beta|\rangle_{mn} = \frac{J_d Q_{mn}}{\sqrt{\pi}},$$

it follows by definition that

$$\langle pv\rangle = \frac{K_d Q_{mn}}{\langle|\beta|\rangle_{mn}}, \quad \text{(A6)}$$

where $K_d = (pv)J_d/\sqrt{\pi}$.

Using this result, it is possible to make use of all spark data points where spark-chamber inefficiencies might otherwise prevent it.

In practice, the situation is complicated by the presence of reading noise which introduces an uncertainty δy in the measured spark position. Defining

$$n_{mn} = [2(m^2 + mn + n^2)]^{1/2}\delta y,$$

the measured $\langle|\beta|\rangle_{mn}$ becomes

$$\langle|\beta|\rangle_{mn} = [(K_d Q_{mn})^2 + n_{mn}^2]^{1/2}.$$

The weighted summation of the combined readings of different combinations of all lengths must be done with careful consideration of the statistics and the significance of the scattering signal. The method chosen for SAS-2 analysis is given by

$$\frac{1}{(pv)} = (\sum\eta_{mn}\omega_{mn})^{-1}\sum\frac{\eta_{mn}\omega_{mn}}{K_d Q_{mn}}(\langle|\beta|\rangle_{mn}^2 - n_{mn}^2)^{1/2}, \quad \text{(A7)}$$

where η_{mn} is the number of readings of type mn and ω_{mn} is a weighting factor defined by

$$\omega_{mn} = \left[\frac{K_d Q_{mn}}{(pv)_c} - n_{mn}\right].$$

The quantity $(pv)_c$ is taken to be the characteristic energy for the particular spark-chamber configuration and is chosen to be 80 MeV for SAS-2.

The reading noise is a function of the angle of the track, with respect to the chamber axis. To correct for this effect, n_{mn} in equation (A7) has been replaced by $n_{mn}(1 + a\langle\phi\rangle_i + b\langle\phi\rangle_i^2)$, where a and b were determined experimentally and $\langle\phi\rangle_i$ is the average projected angle with respect to the vertical in the x or y view, as specified by the subscript i. It was found in the calibration data that a small residual angular correction was necessary for the highest-energy γ-rays, since no set of a or b values satisfied the entire energy range; this correction was applied as a direct multiplying factor at high energies.

REFERENCES

Agrinier, B., Forichon, M., Leray, J. P., Parlier, B., Montmerle, T., Boella, G., Maraschi, L., Sacco, B., Scarsi, L., DaCosta, J. M., and Palmeira, R. 1973, *Proceedings of 13th International Cosmic Ray Conference*, **1**, 8.
Akabane, R. 1966, *Pub. Astron. Soc. Japan*, **18**, 96.
Albats, P., Frye, G. M., Jr., Thomson, G. B., Hopper, V. D., Mace, O. B., Thomas, J. A., and Staib, J. A. 1974, *Nature*, **251**, 400.
Badhwar, G. D., Kaplon, M. F., and Valentine, D. A. 1974, *Ap. and Space Sci.*, **27**, 147.
Bennett, K., Penengo, P., Rochester, G. K., Sanderson, T. R., and Sood, R. K. 1972, *Nature*, **238**, 31.
Bierman, L., and Davis, L. 1960, *Zs. f. Ap.*, **51**, 19.
Bignami, G. F., and Fichtel, C. E. 1974, *Ap. J.* (*Letters*), **189**, L65.
Black, J. M., and Fazio, G. G. 1973, *Ap. J.* (*Letters*), **185**, L7.
Bratolyubova-Tsulukidze, L. I., Grigorov, N. L., Kalinkin, L. F., Melioransky, A. S., Pryakhin, E. A., Savenho, I. A., and Yufarkin, V. Ya. 1971, *Geomagnetism and Aeronomy* (Soviet), **11**, 585.
Bussard, R. 1974, private communication.
Cavallo, G., and Gould, R. J. 1971, *Nuovo Cimento*, **2B**, 77.
Christ, H., Peters, F., Bignami, G. F., Burger, J. J., Hermsen, W., Paul, J. A., Pfeffermann, E., Taylor, B. G., Voges, W. H., and Willis, R. D. 1974, *Nucl. Inst. and Methods*, **116**, 477.
Cowan, J. J., Kafatos, M., and Rose, W. K. 1974, preprint.
Cowsik, R. 1974, *COSPAR Proceedings*, **IIIA**1.4.
Dahlbacka, G. H., Freier, P. S., and Waddington, C. J. 1973, *Ap. J.*, **180**, 371.
Daniel, R. R., Joseph, G., and Lavakare, P. J. 1972, *Ap. and Space Sci.*, **18**, 462.
Dennis, B. R., Suri, A. N., and Frost, K. J. 1973, *Ap. J.*, **186**, 97.
Derdeyn, S. M., Ehrmann, C. H., Fichtel, C. E., Kniffen, D. A., and Ross, R. W. 1972, *Nucl. Instr. and Methods*, **98**, 557.
Duin, R. M., Strom, R. G., and Van der Laan, H. 1973, in *Supernovae and Supernova Remnants*, ed. C. B. Cosmovici (Dordrecht: Reidel), p. 295.
Fichtel, C. E., Hartman, R. C., and Kniffen, D. A. 1973*a*, *Proceedings of 13th International Cosmic Ray Conference*, **1**, 302.
———. 1973*b*, *Ap. J.* (*Letters*), **186**, L99.
Fichtel, C. E., Hartman, R. C., Kniffen, D. A., and Sommer, M. 1972, *Ap. J.*, **171**, 31.
Fichtel, C. E., Kniffen, D. A., and Ögelman, H. B. 1969, *Ap. J.*, **158**, 193.
Frye, G. M., Jr. 1972, summarized by G. G. Fazio in *X- and Gamma-Ray Astronomy*, ed. H. Bradt and R. Giacconi (Dordrecht: Reidel), p. 303.
Frye, G. M., Jr., Albats, P., Thomson, G. B., Hopper, V. D., Mace, O. B., and Thomas, J. A. 1974, *ESLAB Symposium on Gamma Ray Astronomy* (Frascati, Italy).
Frye, G. M., Jr., Albats, P. A., Zych, A. D., Staib, J. A., Hopper, V. D., Rawlinson, W. R., and Thomas, J. A. 1971, *Nature*, **231**, 372.
Frye, G., Jr., Staib, J., Zych, A., Hopper, V., Rawlinson, W., and Thomas, J. 1969, *Nature*, **223**, 1320.
Galper, A. M., Kirillov-Gyryumov, V. G., Luchkov, B. I., and Ozerov, Yu. V. 1973, *Proceedings of 13th International Cosmic Ray Conference*, **1**, 450.
Gamow, G. 1948, *Phys. Rev.*, **74**, 505.
Goldreich, P., and Kwan, J. 1974, *Ap. J.*, **191**, 93.
Goldstein, M. L., Ramaty, R., and Fisk, L. A. 1970, *Phys. Rev. Letters*, **24**, 1193.
Golenetskii, S. V., Mazets, E. P., Il'inskii, V. N., Aptekar', R. L., Bredov, M. M., Gur'yan, Yu. A., and Panov, V. N. 1971, *Ap. Letters*, **9**, 69.
Harrison, E. R. 1967, *Phys. Rev. Letters*, **18**, 1011.
Hartman, R. C., Fichtel, C. E., Kniffen, D. A., Thompson, D. J., Ögelman, H. B., and Tümer, T. 1973, *Proceedings of 13th International Cosmic Ray Conference*, **4**, 2733.
Herterich, W., Pinkau, K., Rothermel, H., and Sommer, M. 1973, *Proceedings of 13th International Cosmic Ray Conference*, **1**, 21.
Hopper, V. D., Mace, O. B., Thomas, J. A., Albats, P., Frye, G. M., Jr., Thomson, G. B., and Staib, J. A. 1973, *Ap. J.* (*Letters*), **186**, L55.
Hutchinson, G. W., Pearce, A. J., Ramsden, D., and Wills, R. D. 1971, *Proceedings of the 11th International Cosmic Ray Conference*, **1**, 87.
Ilovaisky, S. A., and Lequeux, J. 1972, *Astr. and Ap.*, **18**, 169.
Kniffen, D. A. 1969, NASA Tech. Report TR R-308.
Kniffen, D. A., Hartman, R. C., Thompson, D. J., Bignami, G. F., Fichtel, C. E., Ögelman, H., and Tümer, T. 1974, *Nature*, **251**, 397.
Kniffen, D. A., Hartman, R. C., Thompson, D. J., and Fichtel, C. E. 1973, *Ap. J.* (*Letters*), **186**, L105.
Koch, M. W., and Motz, J. W. 1959, *Rev. Mod. Phys.*, **31**, 920.
Kraushaar, W. L., Clark, G. W., Garmire, G. P., Borken, R., Higbie, P., Leong, V., and Thorsos, T. 1972, *Ap. J.*, **177**, 341.
Kuo, Fu-Shong, Frye, G. M., Jr., and Zych, A. D. 1973, *Ap. J.* (*Letters*), **186**, L51.
Lee, M. A. 1972, *Ap. J.*, **178**, 837.
Mazets, E. P., Golenetskii, S. V., Il'inskii, V. N., Gur'yan, Yu. A., and Kharitonova, T. V. 1974, A. F. Joffe Physico Technical Inst. preprint No. 468.
Moliere, G. 1955, *Zs. f. Naturforschung*, **10a**, 177.
Omnès, R. 1969, *Phys. Rev. Letters*, **23**, 38.
Parker, E. N. 1966, *Ap. J.*, **145**, 811.
———. 1969, *Space Sci. Rev.*, **9**, 654.
Pinkau, K. 1966, *Zs. f. Phys.*, **96**, 163.
———. 1968, Max-Planck-Institut preprint.
Reichley, P. 1974, private communication.
Roberts, W. W., and Yuan, C. 1970, *Ap. J.*, **161**, 887.
Samimi, J., Share, G. H., and Kinzer, R. L. 1974, *ESLAB Symposium on Gamma Ray Astronomy* (Frascati, Italy).
Schlickeiser, R., and Thielheim, K. O. 1974, *Astr. and Ap.*, **34**, 167.
Schonfelder, V., and Lichti, G. 1974, *Ap. J.* (*Letters*), **191**, L1.
Schwartz, D., and Gursky, H. 1973, in *Gamma Ray Astrophysics*, ed. F. W. Stecker and J. I. Trombka (Washington: Government Printing Office), p. 15.
Scoville, N. Z., and Solomon, P. M. 1974, *Ap. J.* (*Letters*), **187**, L67.
———. 1975, to be published in *Ap. J.*
Share, G. H., Kinzer, R. L., and Seeman, N. 1974*a*, *Ap. J.*, **187**, 45.
———. 1974*b*, *ibid.*, **187**, 511.
Simonson, S. C., III. 1970, *Astr. and Ap.*, **9**, 163.
———. 1973, preprint.
Solomon, P. M., and Stecker, F. W. 1974, *ESLAB Symposium on Gamma Ray Astronomy* (Frascati, Italy).
Sood, R. K., Bennett, K., Clayton, P. G., and Rochester, G. N. 1974, *ESLAB Symposium on Gamma Ray Astronomy* (Frascati, Italy).
Stecker, F. W. 1969, *Ap. J.*, **157**, 507.
———. 1970, *Ap. and Space Sci.*, **6**, 377.
———. 1973, *Ap. J.*, **185**, 499.
Stecker, F. W., Morgan, D. L., and Bredekamp, J. 1971, *Phys. Rev. Letters*, **27**, 1469.
Stecker, F. W., Puget, J. L., Strong, A. W., and Bredekamp, J. H. 1974, *Ap. J.* (*Letters*), **188**, L59.
Strong, A. W., Wdowczyk, J., and Wolfendale, A. W. 1973, in *Gamma Ray Astrophysics*, ed. F. W. Stecker and J. I. Trombka (Washington: Government Printing Office), p. 239.
Thielheim, K. O., and Langhoff, W. 1968, *J. Phys. A* (*Proc. Phys. Soc.*), Ser. 2, **1**, 694.
Thompson, D. J., Bignami, G. F., Fichtel, C. E., and Kniffen, D. A. 1974, *Ap. J.* (*Letters*), **190**, L15.
Townsend, M. R. 1969, NASA Technical Note TND-5099.
Trombka, J. I. 1974, private communication.
Trombka, J. I., Metzger, A. E., Arnold, J. R., Matteson, J. L., Reedy, R. C., and Peterson, L. E. 1973, *Ap. J.*, **181**, 737.
Trombka, J. I., and Schmadebeck, R. L. 1968, NASA SP-3044.
Vedrenne, G., Albernhe, F., Martin, I., and Talon, R. 1971, *Astr. and Ap.*, **15**, 50.

Volobuyev, S. A., Galper, A. M., Iyudin, A. F., Kirillov-Ugryumov, V. G., Luchkov, B. I. and Ozerov, Yu. V. 1971, *Proceedings of 12th International Cosmic Ray Conference.*
Wentzel, D. G. 1974, *Ann. Rev. Astr. and Ap.*, **12**, 71.
Winkler, P. F., and Clark, G. W. 1974, *Ap. J.* (*Letters*), **191**, L67.
Wolfendale, A. W. 1974, Royal Society Discussion Meeting (Feb.).

G. F. Bignami, C. E. Fichtel, R. C. Hartman, D. A. Kniffen, and D. J. Thompson: Code 662, NASA/Goddard Space Flight Center, Greenbelt, MD 20771

H. Ögelman, M. F. Özel, and T. Tümer: Physics Department, Middle East Technical University, Ankara, Turkey